Valence Bands Convergence in p-Type $CoSb_3$ through Electronegative Fluorine Filling

Xiege Huang(黄写格)[1†], Jialiang Li(李家良)[2†], Haoqin Ma(马浩钦)[1], Changlong Li(李昌隆)[1], Tianle Liu (刘天乐)[1], Bo Duan (段波)[1*], Pengcheng Zhai(翟鹏程)[1,3], and Guodong Li(李国栋)[1,3*]

[1]*Hubei Key Laboratory of Theory and Application of Advanced Materials Mechanics, Wuhan University of Technology, Wuhan 430070, China*
[2]*School of Civil Engineering & Architecture, Wuhan Polytechnic University, Wuhan 430023, China*
[3]*State Key Laboratory of Advanced Technology for Materials Synthesis and Processing, Wuhan University of Technology, Wuhan 430070, China*

(Received 15 April 2024; accepted manuscript online 19 June 2024)

Band convergence is considered to be a strategy with clear benefits for thermoelectric performance, generally favoring the co-optimization of conductivity and Seebeck coefficients, and the conventional means include elemental filling to regulate the band. However, the influence of the most electronegative fluorine on the $CoSb_3$ band remains unclear. We carry out density-functional-theory calculations and show that the valence band maximum gradually shifts downward with the increase of fluorine filling, lastly the valence band maximum converges to the highly degenerated secondary valence bands in fluorine-filled skutterudites. The effective degeneracy near the secondary valence band promotes more valleys to participate in electric transport, leading to a carrier mobility of more than the threefold and nearly twofold effective mass for $F_{0.1}Co_4Sb_{12}$ compared to Co_4Sb_{12}. This work provides a new and promising route to boost the thermoelectric properties of p-type skutterudites.

DOI: 10.1088/0256-307X/41/7/077102

Thermoelectric (TE) semiconductors have the potential to directly realize reversible conversion of heat and electricity via driving the directional migration of charge carriers, which are expected to be applied in waste heat utilization and micro-cooling.[1,2] The TE conversion efficiency is typically expressed as a dimensionless figure of merit $ZT = \alpha^2\sigma T/\kappa$. Thus, an excellent TE semiconductor requires high Seebeck coefficient α, high electrical conductivity σ, and low total thermal conductivity κ.[3] A series of effective strategies for tuning electrical and thermal transport properties have been proposed, including band structure engineering to optimize electrical transport performance,[4] multi-scale defects to suppress κ[5] and magnetoelectric interaction to tune transport behaviors.[6,7] In addition, researchers are still working to develop new strategies to improve the properties of thermoelectric materials. For example, Xie *et al.*[8] developed a screening strategy for thermoelectric interface materials based on phase diagram prediction calculated by density functional theory, which combines room-temperature resistivity and melting point criteria to discover more complex interface candidates. Qin *et al.*[9] proposed the grid-plainification strategy, which grew the crystal by physical vapor deposition and added additional Pb to fill the lattice vacancies, greatly weakening the scattering of lattice defects on the carriers and significantly improving the carrier mobility.

Cage-like $CoSb_3$ skutterudites with the concept of "phonon-glass electron crystal"[10] is one of the most promising TE semiconductors in the temperature range of 500–900 K. The n-type $CoSb_3$ has an outstanding electronic band structure at Γ with threefold degeneracy at the conduction band minimum (CBM).[11–13] Moreover, the secondary conduction band in the zone N–Γ with extremely high valley degeneracy and the CBM converge at high temperatures result in extraordinary TE performances.[14] Filling and doping are effective means to regulate band convergence of n-type $CoSb_3$.[15–17] However, p-type $CoSb_3$ only possesses a linear single band at valence band maximum (VBM), resulting in a small carrier effective mass.[18] Although it has a high hole mobility, the Seebeck coefficient decreases faster.[19] Likewise, a secondary valence band exists in zone H–N (with extremely high valley degeneracy), 0.34 eV lower than the VBM.[20] Therefore, valence band convergence also has the potential to improve the TE properties of p-type $CoSb_3$.

Based on molecular orbital theory, bandgap is related to atomic orbital energy difference and bond energy.[21] The theory indicates that the more electronegative difference between constitution elements leads to a wide bandgap. A proper wide bandgap (E_g) is essential to obtain the best TE performance at the best optimal temperature due to the avoidance of intrinsic excitation.[22] For $Yb_yCo_4Sb_{12}$ skutterudites, the secondary conduction band gradually converges downward to CBM with temperature, while the bandgap remains almost stable.[14] Hydrostatic

†These authors contributed equally to this work.
*Corresponding authors. Email: duanboabc@whut.edu.cn; guodonglee@whut.edu.cn
© 2024 Chinese Physical Society and IOP Publishing Ltd

pressure can widen E_g and promote band convergence between the valley band and CBM, which is beneficial to improve the Seebeck coefficient. In contrast, hydrostatic tension diminishes E_g and the valley band near CBM.[20] Thus, shifting the valence band maximum downward, enlarging the bandgap and converging to the secondary valence band will favor high TE.

In this work, we aim to widen the bandgap and achieve band degeneracy for p-type $CoSb_3$. We use density functional theory (DFT) to study the bandgap and band structure of fluorine-filled p-type $CoSb_3$, which has the most electronegativity (3.98) in the periodic table. The results show that fluorine filling can simultaneously regulate the band degeneracy and bandgap width of Co_4Sb_{12}, which is beneficial to the synergistic optimization of electrical conductivity and Seebeck coefficient.

All DFT calculations are performed using the projector-augmented-wave method,[23,24] which is implemented in the Vienna *ab initio* simulation package (VASP).[25] The generalized gradient approximation (GGA) in the form of the Perdew–Burke–Ernzerhof exchange-correlation functional is used for the computation,[26] and $2\times2\times2$ gamma-centered Monkhorst–Pack scheme is used to sample the Brillouin zone. The plane wave cutoff energy is set at 600 eV, and the electron convergence and geometric optimization force criteria are 10^{-6} eV and 10^{-2} eV/Å, respectively. We expanded the Co_4Sb_{12} primitive cell into a $2\times2\times2$ supercell of 128 atoms to calculate the formation energy and band structure. We filled the empty cage of the Co–Sb near-cubic cage of the supercell with 1, 2, 4, and 8 fluorine atoms, respectively. BandUP is used for band unfolding calculation.[27]

The starting materials consist of Co (99.995%), Sb (99.999%) powders, and SbF_3 (99.8%) precursors. Stoichiometric ratios of the powders were well hand mixed in glove box and then cold pressing into cylinders with 4.5 mm in height and 14.4 mm in diameter. $F_{0.1}Co_4Sb_{12}$ compounds were synthesized by the high-pressure hight-temperature method in a cubic multi-anvil apparatus at 2.5 GPa and 873 K for 15 min. The obtained ingots were then crushed, hand ground to fine powders, and consolidated by spark plasma sintering at 813 K soaking for 10 min under 40 MPa.

The Seebeck coefficients and electrical conductivities were obtained by the standard four-probe method under He atmosphere. The Hall coefficients R_H were collected using a thermoelectric and magnetic performance testing system at magnetic field strength sweeping between ±1.5 T. The carrier concentration n_H and mobility μ_H were calculated according to the formulas $n_H = 1/(eR_H)$ and $\mu_H = R_H\sigma$, where e is the charge of an electron. The sound velocities were collected by the pulse-echo method.

Co_4Sb_{12} is a body-centered cubic structure with the space group $Im\bar{3}$ (No. 204). The conventional cell is shown in Fig. 1(a), where the Co atom occupies the 8*c* position and the Sb atom occupies the 24*g* position. The structure contains two typical substructures, a rectangular Sb4-ring formed by four coplanar Sb atoms and a Co–Sb-octahedron formed by Co–Sb bonds. In addition, the Co atoms and part of the Sb atoms make up eight near-cubic cages, six of which are filled with Sb4-rings, and the remaining two cages are empty. Here we fill the empty cage with fluorine, as shown in Fig. 1(b).

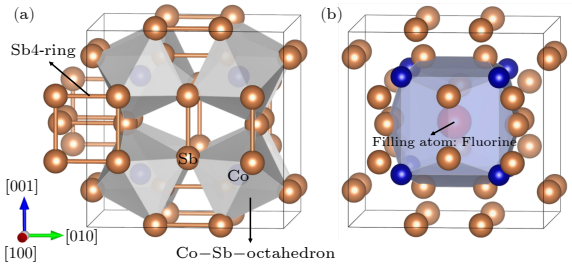

Fig. 1. Crystal structures of (a) $CoSb_3$ skutterudites and (b) $F_{0.5}Co_4Sb_{12}$.

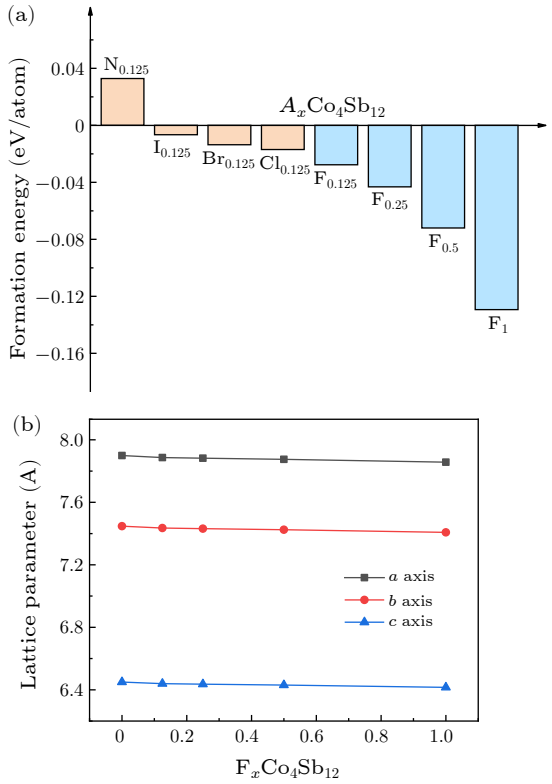

Fig. 2. DFT calculation results: (a) formation energies of $A_xCo_4Sb_{12}$ (A = F, Cl, Br, I, N), (b) lattice parameters of $F_xCo_4Sb_{12}$.

Figure 2(a) depicts the formation energies of $A_xCo_4Sb_{12}$ (A = F, Cl, Br, I, N). It can be found that the N-filled formation energy is positive (0.033 eV/atom), indicating that it is difficult to prepare stable $N_{0.125}Co_4Sb_{12}$. The formation energies of the halogen elements (F, Cl, Br, I) are all negative, thereby the reaction can proceed thermodynamically. It has been demonstrated experimentally that trace amounts of Cl and Br elements have been successfully filled into the cages of Co_4Sb_{12} crystals.[18,19] High pressure can promote the reaction, thereby introducing more Cl elements.[28] Similar tendencies were found in $I_yCo_4Sb_{12}$ and $S_yCo_4Sb_{12-2y}S_{2y}$ skutterudites.[29,30] In Fig. 2(a), it is observed that F-filled Co_4Sb_{12} has the low-

est formation energy and it decreases with the increase of filling amount, indicating the thermodynamical possibilities of synthesizing $F_xCo_4Sb_{12}$ compounds. In addition, we find that F-filled Co_4Sb_{12} causes the triaxial lattice parameter to shrink, as shown in Fig. 2(b). This indicates that F filling affects the crystal structure and shortens the chemical bond length. The XRD refinement of Co_4Sb_{12} and $F_{0.1}Co_4Sb_{12}$ samples is shown in Fig. S2 of the Supplementary Material. It can be found that the lattice parameters decrease with the doping F. The electronegativity of F (3.98) is significantly different from that of Sb (2.05), and there is a small orbital overlap between F and Sb. This F–Sb ionic bond interaction reduces the unit cell parameters.

To shed light on the electrical transport properties of F-filled Co_4Sb_{12}, the DFT calculation is deployed to study the bands of $F_xCo_4Sb_{12}$, as depicted in Fig. 3. The Co_4Sb_{12} is direct bandgap semiconductor at Γ with energy gap of $E_g = 0.17$ eV, as shown in Fig. 3(a).[31,32] The energy difference between the valence band maximum (E_{VBM}) and secondary valence band is 0.34 eV, labeled as ΔE_1. Similarly, the energy difference near the secondary valence band is denoted as ΔE_2 and ΔE_3, respectively. The secondary valence bands were disclosed highly degeneracy due to the twelve congruent faces of the rhombic-dodecahedron-shaped Brillouin zone.[20]

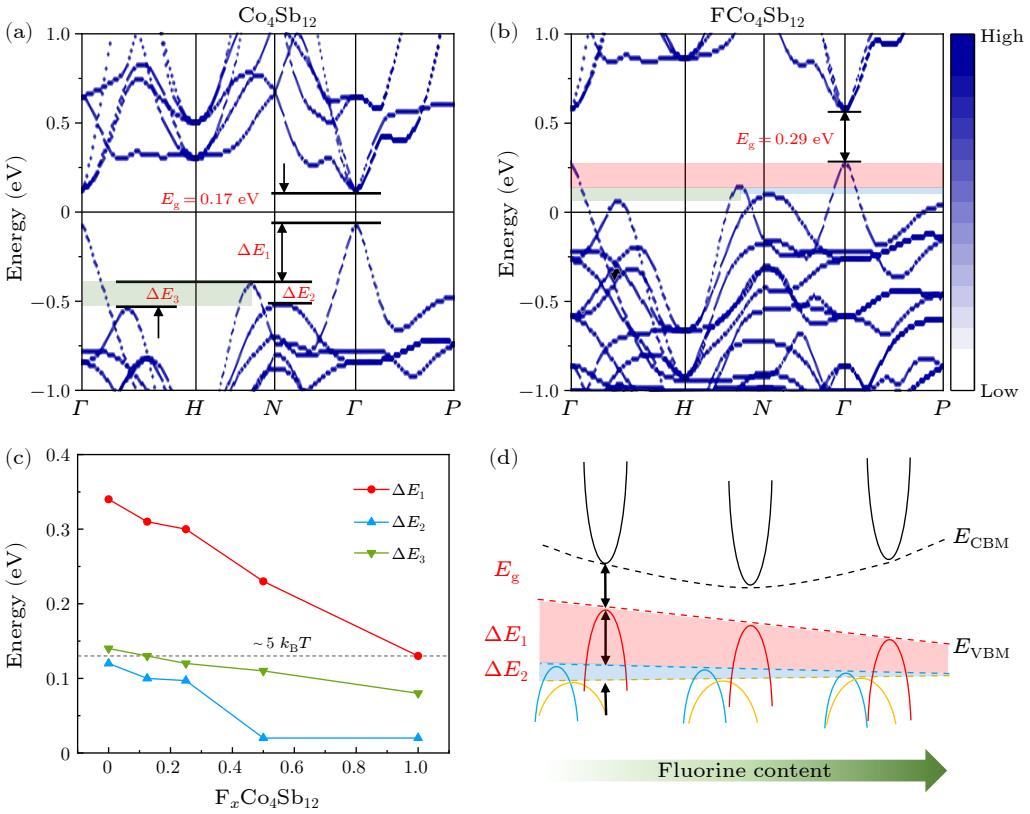

Fig. 3. Band unfolding results: (a) electronic band structures of Co_4Sb_{12}, (b) electronic band structures of FCo_4Sb_{12}, (c) energy difference of $F_xCo_4Sb_{12}$ with filling amount. (d) Schematic diagram of valence band evolution of $F_xCo_4Sb_{12}$ with filling amount.

Moreover, introducing F into the cage vacancy of Co_4Sb_{12} further drives the valence band to achieve band convergence between the VBM and secondary valence band [Fig. 3(b)]. The electronegative guest filling of $R_yCo_4Sb_{12}$ (Br and Cl) is typical of p-type conduction.[19] Similarly, the halogen element F provides holes for the matrix and the Seebeck coefficient of the sample is positive (Table 1), which proves that F acts as a p-type donor. Fluorine filling is a p-type donor, and the Fermi levels of $F_xCo_4Sb_{12}$ are located deeper within the valence band maximum (see Fig. S1 in the Supplementary Material). With the increase of F filling amount, the bandgap of Co_4Sb_{12} first narrows and gradually widens, and increases to 0.29 eV for FCo_4Sb_{12}. However, ΔE_1, ΔE_2, and ΔE_3 monotonically decrease to below $\sim 5k_BT$, achieving effective degeneracy [Fig. 3(c)]. The valence band evolution of $F_xCo_4Sb_{12}$ with the filling amount is shown in Fig. 3(d). The FCo_4Sb_{12} obtains the lowest $\Delta E_1 = 0.13$ eV, leading to the high-valence-band degeneracies of p-type Co_4Sb_{12}.

The element mapping analysis was performed using an electron probe micro-analyzer (EPMA), as shown in Fig. S3 of the Supplementary Material. The backscattered electron image in Fig. S3(a) shows pure phase with uniformly distributed Co [Fig. S3(b)], Sb [Fig. S3(c)] and F [Fig. S3(d)] elements mapping. However, the accuracy of quantitative analysis for light element fluorine (atomic number < 10) is poor.

Then more valence valleys may participate in the

transport of hole carriers, resulting in significantly high carrier mobility for $F_{0.1}Co_4Sb_{12}$ in Table 1. Multiple degenerate valleys also have the effect of producing large effective mass.[4] Table 1 summarizes the electrical transport properties of binary Co_4Sb_{12} and electronegativity (F, Cl, S) doped Co_4Sb_{12} at 300 K. The relationship between electrical properties and temperature of Co_4Sb_{12} and $F_{0.1}Co_4Sb_{12}$ is shown in Fig. S4 of the Supplementary Material. The electrical conductivity of the F filled sample increases first and then decreases with the increase of temperature, and the inflection point is in the temperature range of 475 K–525 K. At low temperature, the increase of electrical conductivity may be due to the increase of carrier concentration by intrinsic excitation. At high temperatures, the decrease in electrical conductivity may be due to bipolar diffusion, and some electrons and holes are neutralized. The α and σ of $F_{0.1}Co_4Sb_{12}$ are simultaneously enhanced greatly. The n_H of $F_{0.1}Co_4Sb_{12}$ remains nearly stable and the μ_H reaches the largest value of $420\,cm^2{\cdot}V^{-1}{\cdot}s^{-1}$. For $Cl_{0.1}Co_4Sb_{12}$, the n_H obtains $38.9 \times 10^{18}\,cm^{-3}$, nearly one order of magnitude larger than Co_4Sb_{12}. Based on the carrier concentrations and Seebeck coefficients, the carrier effective masses are calculated. The carrier effective masses in $F_{0.1}Co_4Sb_{12}$ and $Cl_{0.1}Co_4Sb_{12}$ are, respectively, about twofold and half the value in binary Co_4Sb_{12}. For degenerate semiconductors, the α can be expressed as[4]

$$\alpha = \frac{8\pi^2 k_B T}{3qh^2} m^* \left(\frac{\pi}{3n}\right)^{2/3},$$

where k_B, T, q, h, m^*, and n stand for Boltzmann's constant, absolute temperature in Kelvin, carrier charge, Planck constant, carrier effective mass and carrier concentration, respectively. Consequently, the larger carrier concentration and smaller effective mass of $Cl_{0.1}Co_4Sb_{12}$ are detrimental to the Seebeck coefficient. For $F_{0.1}Co_4Sb_{12}$, since effective mass greatly increases, its Seebeck coefficient becomes larger.

The electrical properties of electronegative S-doped $S_{0.07}Co_4Sb_{11.86}S_{0.14}$ are also listed to compare to $F_{0.1}Co_4Sb_{12}$ in Table 1. Both of them reach considerable electrical conductivity, Seebeck coefficient, carrier concentration, and effective mass. The biggest difference is carrier mobility, i.e., the μ_H of $F_{0.1}Co_4Sb_{12}$ is more than tenfold larger than $S_{0.07}Co_4Sb_{11.86}S_{0.14}$ (only $34\,cm^2{\cdot}V^{-1}{\cdot}s^{-1}$). The low carrier mobility of $S_{0.07}Co_4Sb_{11.86}S_{0.14}$ is attributed to the band flattening, dampening the carrier movement.[21]

Table 1. Electrical conductivity, Seebeck coefficient, power factor, carrier concentration, carrier mobility, and carrier effective mass of Co_4Sb_{12},[30] $F_{0.1}Co_4Sb_{12}$, $Cl_{0.1}Co_4Sb_{12}$,[28] and $S_{0.07}Co_4Sb_{11.86}S_{0.14}$[30] at 300 K.

Samples	Electrical conductivity σ ($10^4\,S{\cdot}m^{-1}$)	Seebeck coefficient α ($\mu V{\cdot}K^{-1}$)	Power factor $\alpha^2\sigma$ ($10^{-3}\,W{\cdot}mK^{-2}$)	Carrier concentration n_H ($10^{18}\,cm^{-3}$)	Carrier mobility μ_H ($cm^2{\cdot}V^{-1}{\cdot}s^{-1}$)	Carrier effective mass m^*/m_e
Co_4Sb_{12}	0.90	92.48	0.08	4.9	121	0.13
$F_{0.1}Co_4Sb_{12}$	3.00	145.13	0.63	5.0	420	0.22
$Cl_{0.1}Co_4Sb_{12}$	11.04	20.30	0.04	38.9	190	0.06
$S_{0.07}Co_4Sb_{11.86}S_{0.14}$	1.12	139.20	0.22	7.0	34	0.26

Table 2. Transverse wave velocity, longitudinal wave velocity, mean sound velocity, elastic modulus, and Poisson's ratio of Co_4Sb_{12},[30] $F_{0.1}Co_4Sb_{12}$, and $S_{0.07}Co_4Sb_{11.86}S_{0.14}$[30] at room temperature.

Samples	Transverse wave velocity v_t (m/s)	Longitudinal wave velocity v_l (m/s)	Mean sound velocity v (m/s)	Elastic modulus E (GPa)	Poisson's ratio υ
Co_4Sb_{12}	2746.3	4700.9	3045.7	137.7	0.24
$F_{0.1}Co_4Sb_{12}$	2741.2	4784.5	3045.3	138.0	0.26
$S_{0.07}Co_4Sb_{11.86}S_{0.14}$	2664.9	4265.8	2935.8	124.5	0.18

The elastic modulus and Poisson's ratio of binary Co_4Sb_{12}, $F_{0.1}Co_4Sb_{12}$, and $S_{0.07}Co_4Sb_{11.86}S_{0.14}$ are derived from the measured sound velocity[33] and summarized in Table 2. Poisson's ratio υ is small ($\upsilon = 0.1$) for covalent materials, whereas for ionic materials a typical value of υ is 0.25.[34] Compared to $S_{0.07}Co_4Sb_{11.86}S_{0.14}$, the sound velocities and elastic modulus of $F_{0.1}Co_4Sb_{12}$ remain stable with Co_4Sb_{12}. Because the electronegativity of fluorine is high, weak ionic F–Sb bonds are formed. The F–Sb bonding energy has little effect on the modulus of $F_{0.1}Co_4Sb_{12}$. The slightly higher Poisson ratio ($\upsilon = 0.26$) also hints at the ionic contribution in F-filled Co_4Sb_{12}. The Gruneisen constant of $F_{0.1}Co_4Sb_{12}$ (1.53) and Co_4Sb_{12} (1.46) have little change ($< 5\%$), indicating that the influence of F filler on the anharmonic vibration of Co_4Sb_{12} is not significant. Therefore, we believe that F filler has little effect on sound velocity. In addition, Fig. S5 shows the thermal conductivity and lattice thermal conductivity of $F_{0.1}Co_4Sb_{12}$ as a function of temperature. Due to the ionic properties of the F–Sb chemical bond, the effect of F on the lattice vibration of the matrix is not significant, and the thermal conductivity of the F-filled sample is close to that of pure Co_4Sb_{12}.

In summary, the most electronegative element fluorine-filled Co_4Sb_{12} is thermodynamically stable and p-type $F_{0.1}Co_4Sb_{12}$ skutterudites were prepared through the

high-pressure high-temperature method. The F-filled Co_4Sb_{12} drives the valence band to achieve band convergence between the valence band maximum and secondary valence band, and FCo_4Sb_{12} bandgap widens to 0.29 eV. The energy difference (ΔE_1, ΔE_2, and ΔE_3) near the secondary valence band drops below $\sim 5k_BT$ with fluorine filling to achieve effective degeneracy, thereby boosting more valence valley participation in the electrical transport. F-filled Co_4Sb_{12} exhibits higher electrical transport properties than $Cl_{0.1}Co_4Sb_{12}$ and $S_{0.07}Co_4Sb_{11.86}S_{0.14}$. The electrical conductivity and Seebeck coefficient of $F_{0.1}Co_4Sb_{12}$ are simultaneously enhanced, attributing to higher carrier mobility and larger effective mass. The elastic modulus and Poisson's ratio indicate the ionic F–Sb bonding in F-filled Co_4Sb_{12}. This work provides an effective method to tune the bandgap and band degeneracy by adjusting the high electronegative fluorine filling, which is beneficial to further improvements of p-type skutterudites.

Supplementary Material. See the Supplementary Material for the band unfolding results of $F_{0.125}Co_4Sb_{12}$, $F_{0.25}Co_4Sb_{12}$, and $F_{0.5}Co_4Sb_{12}$. XRD refinement, electron microscope image, electrical properties and thermal conductivity are shown there.

Acknowledgments. This work was supported by the National Natural Science Foundation of China (Grant Nos. 52171220, 92163212, and 92163119), the Research Funding of Wuhan Polytechnic University (Grant No. 2022RZ059), and the National Innovation and Entrepreneurship Training Program for College Students (Grant No. S202310497202).

References

[1] Xie H Y, Zhao L D, and Kanatzidis M G 2024 *Interdisc. Mater.* **3** 5

[2] Yang Y M, Wang X Z, and Zhang W J 2012 *Acta Mech. Sin.* **28** 1644

[3] Yang H J, Wu L Q, Feng X B, Wang H T, Huang X G, Duan B, Li G D, Zhai P C, and Zhang Q J 2024 *Small* **20** 2310692

[4] Pei Y, Shi X, LaLonde A, Wang H, Chen L, and Snyder G J 2011 *Nature* **473** 66

[5] He J and Tritt T M 2017 *Science* **357** eaak9997

[6] Zhao W, Liu Z, Sun Z, Zhang Q, Wei P, Mu X, Zhou H, Li C, Ma S, He D, Ji P, Zhu W, Nie X, Su X, Tang X, Shen B, Dong X, Yang J, Liu Y, and Shi J 2017 *Nature* **549** 247

[7] Zhao W, Liu Z, Wei P, Zhang Q, Zhu W, Su X, Tang X, Yang J, Liu Y, Shi J, Chao Y, Lin S, and Pei Y 2017 *Nat. Nanotechnol.* **12** 55

[8] Xie L, Yin L, Yu Y, Peng G, Song S, Ying P, Cai S, Sun Y, Shi W, Wu H, Qu N, Guo F, Cai W, Wu H, Zhang Q, Nielsch K, Ren Z, Liu Z, and Sui J 2023 *Science* **382** 921

[9] Qin Y, Qin B, Hong T, Zhang X, Wang D, Liu D, Wang Z Y, Su L, Wang S, Gao X, Ge Z H, and Zhao L D 2024 *Science* **383** 1204

[10] Slack G A and Tsoukala V G 1994 *J. Appl. Phys.* **76** 1665

[11] Li X Y, Chen L D, Fan J F, Zhang W B, Kawahara T, and Hirai T 2005 *J. Appl. Phys.* **98** 083702

[12] Zhai P C, Zhao W Y, Li Y, Liu L S, Tang X F, Zhang Q J, and Niino M 2006 *Appl. Phys. Lett.* **89** 052111

[13] Shi X, Yang J, Salvador J R, Chi M, Cho J Y, Wang H, Bai S, Yang J, Zhang W, and Chen L 2011 *J. Am. Chem. Soc.* **133** 7837

[14] Tang Y L, Gibbs Z M, Agapito L A, Li G D, Kim H S, Nardelli Marco?B, Curtarolo S, and Snyder G J 2015 *Nat. Mater.* **14** 1223

[15] Li H, Tang X, Zhang Q, and Uher C 2009 *Appl. Phys. Lett.* **94** 102114

[16] Dahal T, Jie Q, Joshi G, Chen S, Guo C, Lan Y, and Ren Z 2014 *Acta Mater.* **75** 316

[17] Rogl G, Grytsiv A, Rogl P, Peranio N, Bauer E, Zehetbauer M, and Eibl O 2014 *Acta Mater.* **63** 30

[18] Ortiz B R, Crawford C M, McKinney R W, Parilla P A, and Toberer E S 2016 *J. Mater. Chem. A* **4** 8444

[19] Duan B, Yang J, Salvador J R, He Y, Zhao B, Wang S, Wei P, Ohuchi F S, Zhang W, Hermann R P, Gourdon O, Mao S X, Cheng Y, Wang C, Liu J, Zhai P, Tang X, Zhang Q, and Yang J 2016 *Energy Environ. Sci.* **9** 2090

[20] Hu C, Ni P, Zhan L, Zhao H, He J, Tritt T M, Huang J, and Sumpter B G 2018 *Rare Met.* **37** 316

[21] Zeier W G, Zevalkink A, Gibbs Z M, Hautier G, Kanatzidis M G, and Snyder G J 2016 *Angew. Chem. Int. Ed. Engl.* **55** 6826

[22] Xiao Y and Zhao L D 2020 *Science* **367** 1196

[23] Kresse G and Joubert D 1999 *Phys. Rev. B* **59** 1758

[24] Blöchl P E 1994 *Phys. Rev. B* **50** 17953

[25] Kresse G and Furthmüller J 1996 *Phys. Rev. B* **54** 11169

[26] Perdew J P, Burke K, and Ernzerhof M 1996 *Phys. Rev. Lett.* **77** 3865

[27] Medeiros P V C, Stafström S, and Björk J 2014 *Phys. Rev. B* **89** 041407

[28] Xiao C, Li J, Duan B, Yang H, Wang H, Zhou L, Li G, and Zhai P 2022 *Ceram. Int.* **48** 4270

[29] Li X, Xu B, Zhang L, Duan F, Yan X, Yang J, and Tian Y 2014 *J. Alloys Compd.* **615** 177

[30] Li J, Zhang X, Ma H, Duan B, Li G, Yang J, Wang H, Yang H, Zhou L, and Zhai P 2022 *J. Materiom.* **8** 88

[31] Singh D J and Pickett W E 1994 *Phys. Rev. B* **50** 11235

[32] Sofo J O and Mahan G D 1998 *Phys. Rev. B* **58** 15620

[33] Wu Z J, Zhao E J, Xiang H P, Hao X F, Liu X J, and Meng J 2007 *Phys. Rev. B* **76** 054115 [Publisher's Note: *Phys. Rev. B* **76** 059904]

[34] Bannikov V V, Shein I R, and Ivanovskii A L 2007 *Phys. Status Solidi RRL* **1** 89